

## DIRECT SIMULATIONS OF FLOCCULATION IN SEDIMENTING SOLID-LIQUID SUSPENSIONS

**Jos DERKSEN**

Chemical & Materials Engineering, University of Alberta, Edmonton, Alberta, CANADA  
jos@ualberta.ca

### ABSTRACT

Direct simulations of solid particles settling in a Newtonian liquid have been performed. The particles were given an attractive interaction potential which made them aggregate and settle faster. The lattice-Boltzmann method was used to solve the liquid flow in between the uniformly sized spherical particles. An immersed boundary method was applied to impose no-slip at the surfaces of the spheres that are free to move and rotate under the influence of net gravity, resolved hydrodynamic forces, collisions and their interaction potential. Solids volume fractions were in the range 0.12 – 0.32, and Reynolds numbers (based on average superficial slip velocity) went up to order 50. Drag reduction due to aggregation has been correlated with average aggregate size. This correlation is strongly influenced by the Reynolds number and the overall solids volume fraction.

### NOMENCLATURE

$a$  sphere radius  
 $C_D$  drag coefficient  
 $E_{swp}$  depth of square well potential  
 $e$  restitution coefficient  
 $F$  dimensionless drag force  
 $\mathbf{F}$  force vector  
 $\mathbf{f}$  body force (force per unit volume) vector  
 $\mathbf{g}$  gravitational acceleration vector  
 $L, W$  domain dimensions  
 $m_p$  particle mass  
 $n_a, \langle n_a \rangle$  (average) aggregate size  
 $p(n_a)$  aggregate size distribution  
Re Reynolds number  
 $t$  time  
 $U_\infty$  (single sphere) settling velocity  
 $U$  average slip velocity  
 $\mathbf{u}$  fluid velocity vector  
 $\mathbf{u}_p$  particle velocity vector  
 $\Delta$  lattice spacing  
 $\Delta u$  escape velocity of square well potential  
 $\Delta t$  time step  
 $\delta$  width of square well potential  
 $\mu$  friction coefficient  
 $\nu$  kinematic viscosity  
 $\rho, \rho_p, \bar{\rho}$  density (liquid, particle, mixture)  
 $\phi$  solids volume fraction

### INTRODUCTION

Solid particles settling in liquid under the influence of gravity is a topic of research with a long and rich tradition (Stokes, 1901; Richardson & Zaki, 1954; Batchelor, 1972), continuing interest (Ladd, 2002; Guazzelli & Hinch, 2011), and significant practical relevance. The latter not only because of its application for gravity-based separation, but also in view of fluidization which is a common operation for a variety of industrial processes involving fluid-solid contacting and mixing. For small particles settling in liquids with high viscosities, settling rates get very low which often impedes achieving good process efficiency. One way to enhance settling rates is to promote aggregation (“flocculation”) of the particles so that they form aggregates that fall faster through the liquid than the primary particles. Flocculation is usually achieved by adding chemicals (floculants) to the solid-liquid suspension.

The efficiency of a flocculation process depends on the strength and reach of the attractive interparticle forces that bring about aggregation. It also depends on the hydrodynamic conditions, even if the solids settle through a quiescent liquid. For aggregation to happen, particles need to have non-zero relative velocities so that collision can occur after which particles potentially stick together. If, as is the case for the research presented here, the primary particles are big enough not to undergo Brownian motion, relative velocities between particles are the result of different settling velocities for differently sized particles (and/or differently sized aggregates), and of the randomness of the particle configuration that makes the direct environment of each particle different and thus affects its settling velocity.

Relative velocities amongst solids and between fluid and solid not only promote flocculation, they also provide mechanisms for breaking aggregates. Breakage can be the result of hydrodynamic stresses induced by liquid deformation around the aggregates, or the result of collisions that are energetic enough to break bonds between primary particles thereby destabilizing aggregates.

This paper focuses on the interplay between attraction and subsequent aggregation of particles and the disruption of the aggregation process as a result of hydrodynamic effects and collisions. The only driving force for solids as well as fluid motion considered here is gravity in the presence of a density difference between fluid and solid. The means of investigation is numerical simulation with full resolution of the flow and the solid particle motion. It allows us to carefully control the solid-liquid systems. The

solids in the simulations are spheres all having the same size (radius  $a$ ) and density; the spheres will be referred to as primary particles to clearly distinguish them from aggregates. The liquid is Newtonian with uniform density and viscosity. The spheres are attracted to one another as the result of a square-well potential (Smith et al, 1997). This is a simple, two-parameter model (well width and well depth) for attractive interaction.

The goal of this paper is to reveal the interplay of phenomena (fluid flow, collisions, interaction potential) that lead to aggregation and breakage and thus to an aggregate size distribution, and to quantify the enhanced settling of the aggregating suspension. More specifically, we wish to assess what strength of attraction is required to significantly increase settling velocities and how this required strength would depend on the key dimensionless parameters of the suspension: solids volume fraction and Reynolds number(s).

## FLOW SYSTEM

We consider fully periodic, three-dimensional domains of length  $L$  in the  $x$ -direction, and width  $W$  in  $y$  and  $z$ -direction. Gravity points in the negative  $x$ -direction:  $\mathbf{g} = -g\mathbf{e}_x$ . The domains contain incompressible Newtonian liquid (density  $\rho$ , kinematic viscosity  $\nu$ ) and uniformly sized solid spherical particles with radius  $a$  and density  $\rho_p$ . The overall solids volume fraction is recognized as  $\phi$ . Each sphere experiences a net gravity

force  $\mathbf{F}_g = -(\rho_p - \bar{\rho})\frac{4}{3}\pi a^3 g\mathbf{e}_x$ , with  $\bar{\rho} = \phi\rho_p + (1 - \phi)\rho$

the mixture density. In order to balance forces over the periodic domain we apply a uniform body force acting in the positive  $x$ -direction  $\mathbf{f} = (\bar{\rho} - \rho)g\mathbf{e}_x$  (Derksen & Sundaresan, 2007).

The average hydrodynamic force acting on a sphere follows from a force balance over the liquid:

$$\mathbf{F}_h = \mathbf{f} \frac{4}{3}\pi a^3 \left( \frac{1}{\phi} - 1 \right) \mathbf{e}_x. \text{ Note that this equation expresses}$$

the convention for the drag force as e.g. expressed by Van der Hoef et al (2005) among others (Yin & Sundaresan, 2009; Beetstra et al, 2007). The total average force by the fluid on a sphere  $\mathbf{F}_{f \rightarrow s}$  then is the sum of  $\mathbf{F}_h$  and a

contribution from the body force:  $\mathbf{F}_{f \rightarrow s} = \mathbf{F}_h + \mathbf{f} \frac{4\pi}{3} a^3$ . It

can be verified that  $\mathbf{F}_{f \rightarrow s} = \mathbf{F}_h / (1 - \phi)$ . The hydrodynamic

force is usually partitioned into several components: drag force, added mass force, history force, etc. If we assume that  $\phi$  is uniform throughout the domain, then  $\mathbf{F}_h$  is an input parameter to the simulations. The overall result of a simulation then is the volume-average superficial slip velocity between liquid and particles:

$$U \equiv (1 - \phi) \left[ \langle u \rangle - \langle u_p \rangle \right] \text{ with } \langle u \rangle \text{ the } x\text{-velocity averaged}$$

over the fluid volume and  $\langle u_p \rangle$  the  $x$ -velocity averaged over the particle volume. In what follows, overall results will be mostly presented in terms of  $U$  and in terms of the  $x$ -component of  $\mathbf{F}_h$  made dimensionless according to

$$F \equiv \frac{\mathbf{F}_h \cdot \mathbf{e}_x}{6\pi a \nu \rho U}. \text{ In this way we can relate to the extensive}$$

body of research that uses this representation to

characterize hydrodynamic forces in (dense) suspensions (e.g. Wylie et al, 2003; Kandhai et al, 2003; Van der Hoef et al, 2005). We expect the dimensionless force  $F$  to be a function of  $\text{Re} \equiv U 2a/\nu$ , the solids volume fraction  $\phi$ , and the strength of the interparticle interactions that bring about aggregation.

In addition to the Reynolds number as defined above, we also use a Reynolds number based on the steady state settling velocity of a single sphere in an unbounded fluid:  $\text{Re}_\infty \equiv U_\infty 2a/\nu$ , where  $U_\infty$  is determined by a force balance over the sphere falling through the liquid. In this force balance the drag force correlation given by Schiller & Naumann (1933) is used:  $C_D = 24(1 + 0.15\text{Re}_\infty^{0.687})/\text{Re}_\infty$ . In contrast to  $\text{Re}$ ,  $\text{Re}_\infty$  is an input parameter to the simulations.

The spheres directly interact via a square-well potential (Smith et al, 1997) that serves as the model mechanism for aggregation. If two spheres  $i$  and  $j$  approach one another and reach a center-to-center distance  $2(a + \delta)$ , they enter the square well and are considered ‘attached’. At that moment, an amount  $J$  is added instantaneously to the relative radial approach velocity of the two spheres:

$$\tilde{\mathbf{u}}_{pi} = \mathbf{u}_{pi} + \frac{1}{2}J\mathbf{n}, \quad \tilde{\mathbf{u}}_{pj} = \mathbf{u}_{pj} - \frac{1}{2}J\mathbf{n} \quad (1)$$

with  $\mathbf{u}_{pi}, \mathbf{u}_{pj}$  sphere velocities just before entry, and  $\tilde{\mathbf{u}}_{pi}, \tilde{\mathbf{u}}_{pj}$  just after entry of the SqWP, and

$J = \sqrt{(\Delta\mathbf{u}_{ij} \cdot \mathbf{n})^2 + (2\Delta u)^2} + \Delta\mathbf{u}_{ij} \cdot \mathbf{n}$ . The unit vector  $\mathbf{n}$  points from the center of sphere  $i$  to the center of sphere  $j$ ,  $\Delta\mathbf{u}_{ij} \equiv \mathbf{u}_{pj} - \mathbf{u}_{pi}$ , and  $\Delta u$  is the parameter defining the strength of the SqWP (see below). Note that for two approaching spheres  $\Delta\mathbf{u}_{ij} \cdot \mathbf{n} < 0$  and thus  $J = 0$  if  $\Delta u = 0$  (zero momentum addition if the strength of the SqWP is zero).

In energy terms the above implies that upon entering the square well, potential energy is converted in kinetic energy by a total amount  $2E_{swp} = 2\left(\frac{1}{2}m_p(\Delta u)^2\right)$  (with

$m_p = \frac{4}{3}\pi\rho_p a^3$  the mass of one sphere). Since there are

two spheres involved in the process, on average each sphere gains  $E_{swp}$  kinetic energy. Once in each other’s square well the spheres keep moving under the influence of hydrodynamic forces and likely undergo one or more hard-sphere collisions according to the two-parameter model (restitution coefficient  $e$  and friction coefficient  $\mu$ ) proposed by Yamamoto et al (2001).

If two attached spheres move apart and reach the edge of the SqWP – i.e. have a center-to-center distance of  $2(a + \delta)$  – they need sufficient kinetic energy to escape the SqWP: they need a relative radial separation velocity  $\Delta\mathbf{u}_{ij} \cdot \mathbf{n}$  (when the spheres are separating this inner product is positive) of at least  $2\Delta u$ . If they are able to escape, kinetic energy is converted back to potential energy upon escaping. If they are not able to escape they reverse their relative radial velocity at the moment they reach the edge of the square well and stay attached. The square-well potential is thus defined by two parameters: its width  $\delta$

and its energy  $E_{swp}$ . Rather than working with the energy, we will be working with  $\Delta u$  in the remainder of this paper. As indicated, the two are related according to

$$E_{swp} = \frac{1}{2} m_p (\Delta u)^2.$$

This leaves us with four parameters governing direct (as opposed to hydrodynamic) particle-particle interactions. In dimensionless terms these are the collision parameters  $e$  (restitution coefficient) and  $\mu$  (friction coefficient), and the square-well potential parameters  $\delta/a$ , and  $\Delta u/U_\infty$ . In this study we restrict ourselves to fully elastic and smooth (frictionless) collisions so that  $e=1$  and  $\mu=0$ .

## MODELING APPROACH

We use the lattice-Boltzmann (LB) method (Chen & Doolen, 1998; Succi, 2001) to solve for the flow of liquid in between the spheres. The method has a uniform, cubic grid (grid spacing  $\Delta$ ). The specific scheme employed here is due to Somers (1993). The no-slip condition at the spheres' surfaces was dealt with by means of an immersed boundary (or forcing) method (Goldstein et al, 1993; Ten Cate et al, 2002). In this method, the sphere surface is defined as a set of closely spaced points (the typical spacing between points is  $0.7\Delta$ ), not coinciding with lattice points. At these points, the (interpolated) fluid velocity is forced to the local velocity of the solid surface according to a control algorithm. The local solid surface velocity has contributions from translational and rotational motion of the sphere under consideration. Adding up (discrete integration) per spherical particle of the forces needed to maintain no-slip provides us with the (opposite; action equals minus reaction) force the fluid exerts on the spherical particle. Similarly the hydrodynamic torque exerted on the particles can be determined. Forces and torques are subsequently used to update the linear and rotational equations of motion of each spherical particle. It should be noted that having a spherical particle on a cubic grid requires a calibration step, as earlier realized by Ladd (1994). He introduced the concept of a hydrodynamic radius. The calibration involves placing a sphere with a given radius  $a_g$  in a fully periodic cubic domain in creeping flow and (computationally) measuring its drag force. The hydrodynamic radius  $a$  of that sphere is the radius for which the measured drag force corresponds to the expression for the drag force on a simple cubic array of spheres given by Sangani & Acrivos (1982). Usually  $a$  is slightly larger than  $a_g$  with  $a - a_g$  typically equal to half a lattice spacing or less. The simulations presented in this paper have a resolution such that  $a = 6\Delta$ . In previous studies (e.g. Derksen & Sundaresan, 2007) we have confirmed (through grid refinement studies) that this is an appropriate resolution for particle-based Reynolds numbers up to order 50.

Once the spatial resolution is fixed, the temporal resolution of the LB simulations goes via the choice of the kinematic viscosity  $\nu$ . The kinematic viscosities varied between 0.02 and 0.005 in lattice units (space unit is  $\Delta$ , time unit is one time step  $\Delta t$ ) so that for the default resolution ( $a = 6\Delta$ ) the viscous time scale  $a^2/\nu$  corresponds to 1800 to 7200  $\Delta t$ . The convective time scale  $a/U_\infty$  is in the range of 200 to 600  $\Delta t$ .

The viscosity is determined by the value for  $Re_\infty \equiv U_\infty 2a/\nu$  we want to achieve in a specific simulation and by the desire to keep fluid velocities well below the speed of sound of the (compressible) lattice-Boltzmann scheme to achieve approximately incompressible flow. If we set  $U_\infty$  to a value of  $O(0.01)$  the flow is practically incompressible. Once  $a$ ,  $\nu$  and  $U_\infty$  have been set, the value for gravitational acceleration  $g$  is determined so as to actually achieve  $U_\infty$ :

$$g = \frac{3}{8} C_D \frac{\rho}{\rho_p - \rho} \frac{U_\infty^2}{a} \quad \text{with } C_D(Re_\infty) \text{ based on the}$$

Schiller-Naumann correlation.

The fixed-grid simulations involving moderately dense suspensions as discussed here require explicit inclusion of sub-grid lubrication forces for which we follow the procedure suggested by Nguyen & Ladd (2002).

The spheres' equations of linear and rotational motion including resolved and unresolved (i.e. lubrication) forces are integrated according to an Euler forward method. These time-step driven updates are linked with an event-driven algorithm that detects events related to the SqWP and to hard-sphere collisions during the Euler time steps. Three types of events can be distinguished: (1) a hard-sphere collision; (2) two approaching spheres enter one another's SqWP; (3) two spheres that move apart reach a center-to-center distance of  $2(a + \delta)$  and attempt to leave one another's SqWP. Event (3) has two possible outcomes: the spheres detach (if their separating relative velocity is sufficiently high), or do not detach. Once an event is being detected, all particles are frozen and the event is carried out which for all three event types implies an update of the linear velocities (and also angular velocities for event type (1) if  $\mu \neq 0$ ) of the two spheres involved in the event. Subsequently all spheres continue moving until the end of the time step, or until the next event, whatever comes first.

The initial condition is a domain that contains solid and liquid at rest and the (non-overlapping) spheres randomly distributed in the domain. Then gravity is switched on while  $\Delta u = 0$  (inactive SqWP) and the system is evolved to a dynamically stationary state. Once this state has been reached, the strength of the SqWP  $\Delta u$  is set to its desired value and we let the solid-liquid system adapt itself to this new condition.

## DIMENSIONLESS PARAMETERS

Table 1 summarizes the non-dimensional input parameters fully defining the simulations. It also shows which parameters have been set to *fixed* values, which parameters have a *default* value the effect of which has been investigated for a few cases, and which parameters have been *varied* independently (the table then shows the range of variation). As can be seen, we cover part of a three-dimensional parameter space with independently varied coordinates  $\phi$ ,  $Re_\infty$ , and  $\Delta u/U_\infty$ .

Note that a Stokes number can be defined by combining  $Re$  and the (in this study constant) density ratio  $\rho_p/\rho$  to

$$St = \frac{2}{9} \frac{\rho_p}{\rho} Re.$$

parameter	description	status	value /range
$\phi$	solids volume fraction	varied	0.12 – 0.32
$Re_\infty$	single particle settling Reynolds number	varied	6 – 72
$\rho_p/\rho$	density ratio	fixed	4.0
$\Delta u/U_\infty$	SqWP escape velocity over settling velocity	varied	0.005 – 0.030
$\delta/a$	SqWP width over sphere radius $a$	fixed	0.025
$e$	restitution coefficient	fixed	1.0
$\mu$	friction coefficient	fixed	0.0
$L/a$	domain length over $a$	default	48
$L/W$	domain length over domain width	fixed	2

**Table 1:** Dimensionless input parameters defining the simulation cases and their settings

## RESULTS

### Impressions of Aggregating Systems

We begin by presenting some qualitative results. As a metric for the level of aggregation, the average number of sphere-sphere contacts per sphere ( $C_{sph}$ ), i.e. the number of spheres that are within a center-to-center distance of  $2(a + \delta)$  of a certain test sphere, is considered. In Figure 1 we show time series of  $C_{sph}$ . At moment  $t=0$ , when the non-aggregating suspension is in a stationary state, the square-well potential is switched on, i.e. we switch from  $\Delta u=0$  to the values as indicated in the figure. The result is an increase in  $C_{sph}$  to an extent that clearly depends on the strength of the potential. With respect to solids volume fraction  $\phi$  and single-sphere-settling Reynolds number  $Re_\infty$ , the level of aggregation follows to-be-expected trends: denser systems aggregate more, whereas the more vigorous motion and higher (liquid and solids) inertia and associated collision for the higher Reynolds numbers limit aggregation levels. Impressions of sphere configurations for some cases are given in Figure 2. From this figure the size of the simulation domains and the aggregate structures being formed can be gauged.

For  $\phi=0.32$  (the lower panels in Figure 1) and  $\frac{\Delta u}{U_\infty} \geq 0.020$  aggregation gets so strong that eventually a very large aggregate forms that contains almost all primary spheres and has a size of the order of the domain size. In some of these cases (see Figure 1) a steady state is not reached within time  $200a/U_\infty$ . In such situations and given the fully periodic boundary conditions the single, large aggregate interacts with itself and the settling velocity and drag force results are not representative for large, homogeneous systems anymore. For this reason, aggregating systems with  $\phi=0.32$  will not be discussed further.

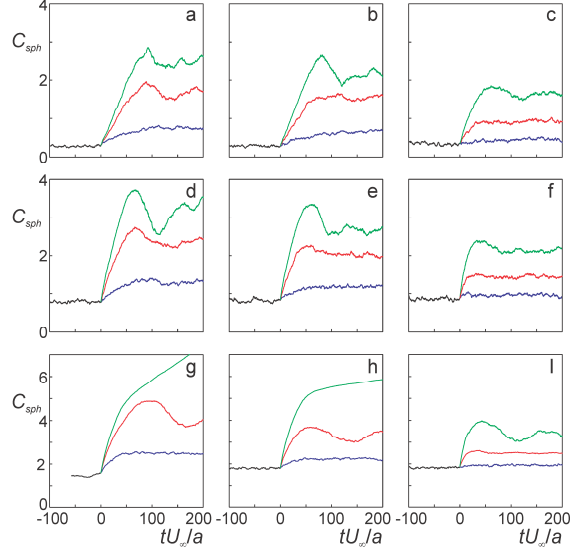


**Figure 1:** Time series of the number of contact points per sphere  $C_{sph}$ . Top row:  $\phi=0.12$ ; middle row:  $\phi=0.20$ ; bottom row:  $\phi=0.32$ . Left column:  $Re_\infty=6$ ; center column:  $Re_\infty=12$ ; right column:  $Re_\infty=48$ . Black:  $\Delta u/U_\infty=0$ ; blue:  $\Delta u/U_\infty=0.01$ ; red:  $\Delta u/U_\infty=0.02$ ; green:  $\Delta u/U_\infty=0.03$ . At  $t=0$   $\Delta u$  switches from zero to the indicated non-zero values.

The square-well potential and consequential flocculation clearly enhances the settling rates, see Figure 3. The more remarkable feature of the results in this figure is that the enhancement of settling is a very strong function of  $Re_\infty$ . For the higher  $Re_\infty$  (and thus higher Stokes numbers; note that the density ratio is constant in this work), inertia promotes collisions that potentially break aggregates and keeps the spheres less attached. The result is a somewhat more uniform distribution of particles with quite drastic consequences for the settling rates.

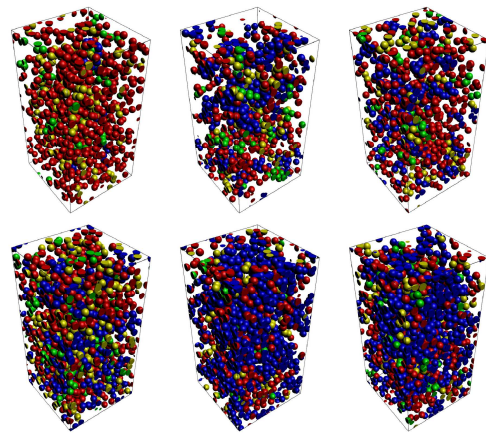


**Figure 2:** Single realizations of sphere positions under stationary conditions. Top row  $\phi=0.12$ ; bottom row  $\phi=0.20$ . Left  $Re_\infty=6$  and  $\Delta u/U_\infty=0$ ; middle:  $Re_\infty=6$  and  $\Delta u/U_\infty=0.03$ ; right  $Re_\infty=48$  and  $\Delta u/U_\infty=0.03$ . Red are single spheres, green spheres are part of doublets, yellow spheres are part of triplets, and blue spheres are in aggregates of four or more primary spheres.

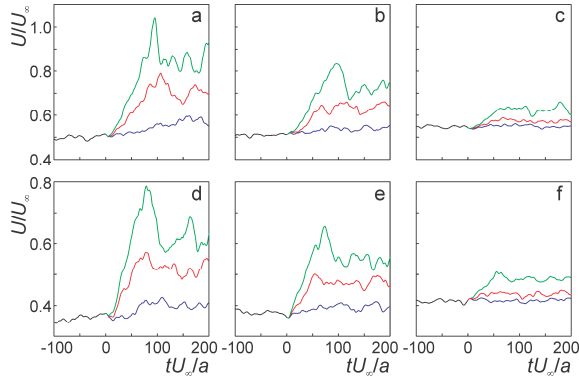


**Figure 3:** Time series of sphere-averaged slip velocity  $U$  normalized with  $U_\infty$ . Top row:  $\phi=0.12$ ; bottom row:  $\phi=0.20$ . Left column:  $Re_\infty=6$ ; center column:  $Re_\infty=12$ ; right column:  $Re_\infty=48$ . Black:  $\Delta u/U_\infty=0$ ; blue:  $\Delta u/U_\infty=0.01$ ; red:  $\Delta u/U_\infty=0.02$ ; green:  $\Delta u/U_\infty=0.03$ .

### Drag in Aggregating Systems

Aggregate size distributions (ASD's) were determined based on a large number of realizations of the aggregating solid-liquid systems after they reached a dynamic steady state. Examples of mass-weighted ASD's are presented in Figure 4. In this figure,  $p(n_a)$  is the fraction of the total solids mass in the system contained in aggregates consisting of  $n_a$  primary spheres. Figure 4 shows that a stronger interaction potential shifts the ASD's to the right, i.e. to (on average) larger aggregates. Given the definition of  $p(n_a)$ , the mass-averaged aggregate size is  $\langle n_a \rangle \equiv \sum_{n_a=1}^N n_a p(n_a)$  with  $N$  the number of primary spheres in the entire flow system ( $N$  is the absolute upper limit of  $n_a$ ). In Figure 5 mass averaged aggregate sizes are given as a function of the three independent input variables  $\phi$ ,  $Re_\infty$ , and  $\Delta u/U_\infty$ .

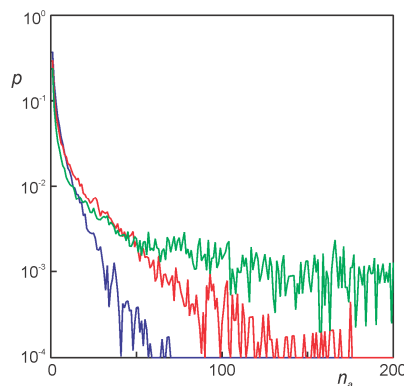


**Figure 4:** Aggregate size distributions for  $\phi=0.20$  and  $Re_\infty=12$ . Blue:  $\Delta u/U_\infty=0.01$ ; red:  $\Delta u/U_\infty=0.02$ ; green:  $\Delta u/U_\infty=0.03$ . The mass-weighted averages are  $\langle n_a \rangle = 4.88, 11.9, \text{ and } 59.4$  respectively. The total number of particles in each case is 1320. The ASD's are based on 600 realizations after steady state was reached.  $p$ -values below  $10^{-4}$  have been set to  $10^{-4}$  (for plotting purposes only).

As expected, there is a clear positive correlation between aggregate size and interaction potential strength and solids volume fraction. A slightly less obvious observation is that higher  $Re_\infty$  (i.e. an increase of inertia) drastically brings down average aggregate sizes. The reason for this effect is that inertia promotes the number and intensity of particle-particle collisions that tend to destabilize and break aggregates, thereby shifting the size distribution towards smaller aggregates. It should be noted that the results for  $\phi=0.25$  and  $\frac{\Delta u}{U_\infty} \geq 0.025$  likely are affected by the finite

domain size, given that the mass-averaged aggregate sizes (order a few hundred) are a significant fraction of the total number of spheres (1645) in these simulations so that only a few large aggregates can coexist at one moment in time. In Figure 6 the consequences of aggregation for the drag force are summarized. We show the average drag on a primary sphere under different aggregation conditions.

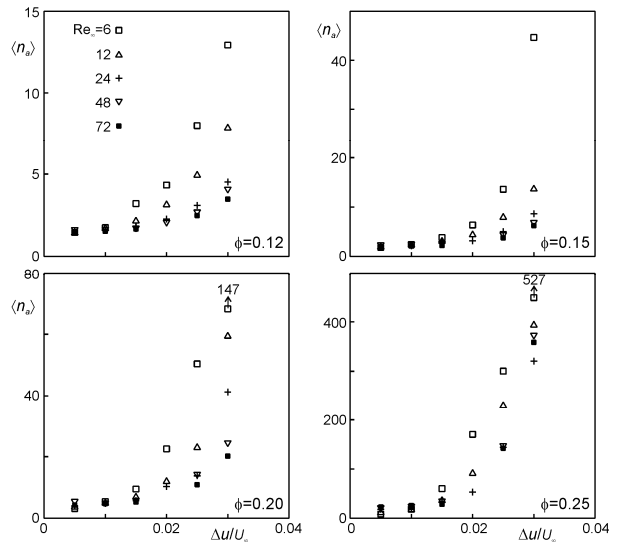


**Figure 5:** Mass-average aggregate size  $\langle n_a \rangle$  as a function of suspension properties.

The drag per primary sphere reduces most for the lower Reynolds numbers which (see Figure 5) aggregate most. There is, however, no one-on-one relation between aggregate size and drag reduction. (1) Although the amount of drag reduction for simulations with  $\phi=0.12$  and  $\phi=0.25$  are comparable, the aggregates in the latter cases are more than one order of magnitude larger than in the former. (2) Aggregates are being formed for the higher Reynolds numbers. Drag, however, is only marginally reduced in these cases.

### SUMMARY

Simulations of flocculating solids settling through liquid were presented with the aim to quantify the per-primary-particle reduction of the average drag force as a result of the aggregation process. The simulations explicitly resolved the no-slip conditions at solid particle surfaces, the flow of interstitial liquid and the solid-particle dynamics, including hard-sphere collisions. The tendency to aggregate was derived from providing the spherical particles with an attractive square-well interaction potential. Minimal modeling was required: a radial lubrication force was added to the particles' equations of

motion to compensate for the lack of resolution when particle surfaces come very close, and a hydrodynamic radius calibration was applied to account for artifacts related to representing spherical surfaces on a cubic lattice.

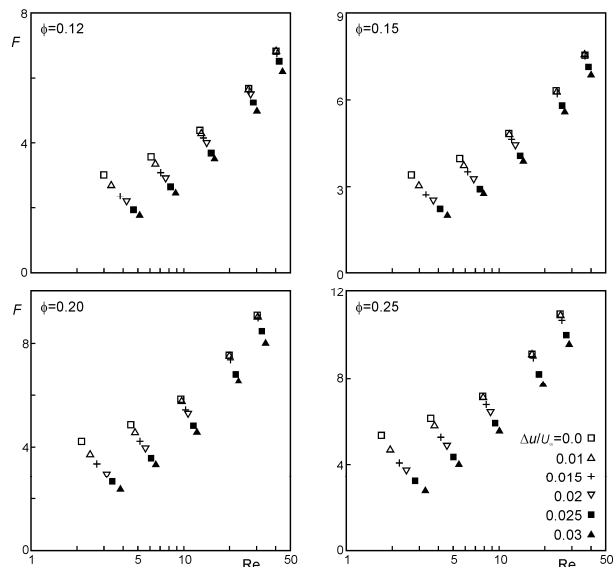


**Figure 6:** Dimensionless drag force per primary sphere ( $F$ ) as a function of  $Re$  for four different solids volume fraction  $\phi$  and SqWP strength  $\Delta u$  (relative to  $U_\infty$ ).

Settling rates clearly increase if the particles aggregate. These increased rates have been interpreted in terms of per-sphere drag reduction. For given overall solids volume fraction, the per-sphere drag reduction mainly depends on the strength of the interaction potential and on the level of inertia present in the system (as a metric for the latter the single-sphere settling Reynolds number  $Re_\infty$  was chosen). The effect of inertia could be traced back to the aggregate sizes that are much smaller for higher  $Re_\infty$  as a result of enhanced collision rates that destabilize large aggregates. Future work will focus on a better understanding and more universal ways to describe and possibly predict enhanced settling through aggregation as a function of the input parameters (solids volume fraction, Reynolds numbers, interaction strength). In addition, the sensitivity of the results with respect to the specifics of the interaction potential needs to be tested. One way to approach this is to mimic experimentally observed potentials and simulate systems that are amenable to experimental testing. From a more practical standpoint we plan in the simulations to include the transport of a flocculant (e.g. a polymer) in the suspension and make the interaction potential dependent on its local concentration. In dense suspensions the spreading of a scalar through the liquid phase is a significant mixing problem and a rate limiting step in large scale flocculation processes.

## REFERENCES

BATCHELOR, G.K., (1972), "Sedimentation in a dilute dispersion of spheres", *J. Fluid Mech.*, **52**, 245-268.  
 BEETSTRA, R., VAN DER HOEF, M.A. and KUIPERS, J.A.M., (2007), "Drag force of intermediate Reynolds number

flows past mono- and bidisperse arrays of spheres", *AIChE J.*, **53**, 489-501.

CHEN, S. and DOOLEN, G.D., (1998), "Lattice-Boltzmann method for fluid flows", *Annu. Rev. Fluid Mech.*, **30**, 329-364.

DERKSEN, J.J. and SUNDARESAN, S., (2007), "Direct numerical simulations of dense suspensions: wave instabilities in liquid-fluidized beds", *J. Fluid Mech.*, **587**, 303-336.

GOLDSTEIN, D., HANDLER, R. and SIROVICH, L., (1993), "Modeling a no-slip flow boundary with an external force field", *J. Comp. Phys.*, **105**, 354-366.

GUZZELLI, É. and HINCH, J., (2011), "Fluctuations and instability in sedimentation", *Annu. Rev. Fluid Mech.*, **43**, 97-116.

KANDHAI, D., DERKSEN, J.J. and VAN DEN AKKER, H.E.A., (2003), "Interphase drag coefficients in gas-solid flows", *AIChE J.*, **49**, 1060-1065.

LADD, A.J.C., (1994) "Numerical simulations of particle suspensions via a discretized Boltzmann equation. Part I: Theoretical Foundation", *J. Fluid Mech.*, **271**, 285-309.

LADD, A.J.C., (2002), "Effect of container walls on the velocity fluctuations of sedimenting spheres", *Phys. Rev. Lett.*, **88**, 048301.

NGUYEN, N.-Q. and LADD, A.J.C., (2002), "Lubrication corrections for lattice-Boltzmann simulations of particle suspensions", *Phys. Rev. E*, **66**, 046708.

RICHARDSON, J.F. and ZAKI, W.N., (1954), "The sedimentation of a suspension of uniform spheres under conditions of viscous flow", *Chem. Engng. Sc.*, **8**, 65-73.

SANGANI, A.S. and ACRIVOS, A., (1982) "Slow flow through a periodic array of spheres", *Int. J. Multiphase Flow*, **8**, 343-360.

SCHILLER, L. and NAUMANN, A., (1933) "Über die grundlegenden Berechnungen bei der Schwerkraftaufbereitung", *Ver. Deut. Ing. Z.*, **77**, 318-320.

SMITH, S.W. HALL, C.K. and FREEMAN, D.B., (1997), "Molecular dynamics for polymeric fluids using discontinuous potentials", *J. Comp. Phys.*, **134**, 16-30.

SOMERS, J.A., (1993), "Direct simulation of fluid flow with cellular automata and the lattice-Boltzmann equation", *App. Sci. Res.*, **51**, 127-133.

STOKES, G.G., (1901), *Mathematical and Physical Papers, Volumes I-V*. Cambridge University Press.

SUCCI, S., (2001), *The lattice Boltzmann equation for fluid dynamics and beyond*. Clarendon Press, Oxford.

TEN CATE, A., NIEUWSTAD, C.H., DERKSEN, J.J. and VAN DEN AKKER, H.E.A., (2002), "PIV experiments and lattice-Boltzmann simulations on a single sphere settling under gravity", *Phys. Fluids*, **14**, 4012-4025.

VAN DER HOEF, M.A., BEETSTRA, R. and KUIPERS, J.A.M., (2005), "Lattice-Boltzmann simulations of low-Reynolds-number flow past mono- and bidisperse arrays of spheres: results for the permeability and drag force", *J. Fluid Mech.*, **528**, 233-254.

WYLIE, J.J., KOCH, D.L. and LADD, A.J.C., (2003), "Rheology of suspensions with high particle inertia and moderate fluid inertia", *J. Fluid Mech.*, **480**, 95-118.

YAMAMOTO, Y., POTTHOFF, M., TANAKA, T., KAJISHIMA, T. and TSUJI, Y., (2001), "Large-eddy simulation of turbulent gas-particle flow in a vertical channel: effect of considering inter-particle collisions", *J. Fluid Mech.*, **442**, 303-334.

YIN, X. and SUNDARESAN, S., (2009), "Drag law for bidisperse gas-solid suspensions containing equally sized spheres", *Ind. Eng. Chem. Res.*, **48**, 227-241.